International Journal of Hydrogen Energy 212 (2026) 153692

Contents lists available at ScienceDirect

International Journal of Hydrogen Energy

journal homepage: www.elsevier.com/locate/he

# Tuning hydrogen adsorption through synergy in non-noble bimetallic substrates

Pedro Ivo R. Moraes [a], Rafael L.H. Freire [a], Marina Medina [b], Juliana F. Brito [b], Lucia H. Mascaro [c], Juarez L.F. Da Silva [a,*]

[a] São Carlos Institute of Chemistry, University of São Paulo, Av Trabalhador São-Carlense 400, 13560-970, São Carlos, SP, Brazil
[b] Institute of Chemistry, São Paulo State University (UNESP), Rua Francisco Degni, 55, Bairro Quitandinha, Araraquara, SP 14800-900, Brazil
[c] Department of Chemistry, Federal University of São Carlos, Rod. Washington Luiz, km 235, 13565-905, São Carlos, São Paulo, Brazil

ARTICLE INFO

*Keywords:*
Computational electrocatalysis
Non-noble transition-metal alloys
Synergistic effects
Hydrogen evolution reaction
Density functional theory calculations

ABSTRACT

The rational design of non-noble transition-metal bimetallic substrates represents a promising approach for developing efficient and tunable electrocatalysts for the hydrogen evolution reaction. In this work, we employ density functional theory calculations with van der Waals corrections combined with the computational hydrogen electrode model to investigate how hydrogen–substrate interactions govern the Gibbs free energy of hydrogen adsorption ($\Delta G_{H^*}$) on ordered bimetallic surfaces. We investigated ordered bimetallic compounds FeNi, FeCu, and NiCu with varying atomic ratios (3:1, 1:1, and 1:3) to establish adsorption-site environment activity relationships. Our results reveal that FeNi exhibits a nearly linear dependence between $\Delta G_{H^*}$ and the substrate ratio, showing that the catalytic activity changes by controlling the ratio of the transition-metal species. This linear scaling behavior provides a predictive framework for the rational design of experiments aimed at improving hydrogen adsorption energetics, which are governed by modulation control of the chemical species directly interfacing with the reaction environment. In contrast, although FeCu and NiCu compounds do not exhibit a linear trend as a function of specific ratios due to the local environment at the adsorption sites, the $FeCu_3$(112) and $NiCu_3$(111) substrates still demonstrate favorable activity. Moreover, hydrogen exhibits a strong energetic preference for hollow sites, where the adsorption energy, the dominant contribution to the Gibbs free energy, correlates directly with the chemical identity of the local catalytic site environment.

## 1. Introduction

The increasing global demand for energy, combined with the escalating environmental crisis, requires urgent advances in renewable and sustainable technologies. These technologies should provide clean and reliable alternatives to fossil fuels while minimizing carbon emissions as much as possible [1]. Promising strategies for sustainable energy conversion include transforming abundant molecules such as water ($H_2O$), carbon dioxide ($CO_2$), and nitrogen ($N_2$), into high-value-added chemicals using renewable energy sources such as solar and wind [2]. Among these approaches, molecular hydrogen ($H_2$) stands out as a clean, high-energy-density carrier and an efficient alternative to carbon-based fuels [3]. However, most current hydrogen production still relies on steam methane reforming, a process dependent on fossil fuels that generates significant $CO_2$ emissions, in contrast to global sustainability goals [4].

Water electrolysis (WE) has emerged as a greener method for producing high-purity hydrogen with a minimal carbon footprint [5]. This chemical process involves two half-reactions: the oxygen evolution reaction (OER) at the anode and the hydrogen evolution reaction (HER) at the cathode. In principle, HER is thermodynamically favorable at 0 V versus the standard hydrogen electrode (SHE). However, kinetic barriers arising from electrode polarization require highly active and stable electrocatalysts to achieve efficient hydrogen production [6]. Currently, platinum-based catalysts are the most efficient materials for HER, but their high cost and scarcity can severely limit large-scale applications in the future [7]. Consequently, efforts have been increasingly directed towards non-noble transition metals (TM) such as Fe, Ni and Cu. Their abundance, tunable electronic properties, and good catalytic performance make them promising candidates as sustainable electrocatalysts [8]. Combining or alloying these TMs with

*Abbreviations:* DFT, Density Functional Theory; PBE, Perdew–Burke–Ernzerhof; VASP, Vienna *Ab initio* Simulation package; PAW, Projector augmented-wave; CHE, Computational Hydrogen Electrode; HER, Hydrogen Evolution Reaction

* Corresponding author.
*E-mail address:* juarez_dasilva@iqsc.usp.br (J.L.F. Da Silva).

https://doi.org/10.1016/j.ijhydene.2026.153692
Received 14 October 2025; Received in revised form 19 December 2025; Accepted 23 January 2026
Available online 29 January 2026

small amounts of noble metals, such as Pt, has proven effective in reducing catalyst costs while preserving high catalytic activity [9,10].

In particular, bimetallic TM alloys exhibit synergistic effects that enhance electronic conductivity, surface reactivity, and long-term stability, all of which are critical for efficient water electrolysis [11]. From an electronic standpoint, the *d*-orbitals filling of TMs plays a pivotal role in proton adsorption and activation during HER [12]. Empty or low-occupancy *d*-states can accept electron density from the hydrogen *s*-orbital during adsorption, forming metal–hydrogen bonds that govern reaction kinetics. Alloying provides a means to engineer these electronic states, thus tailoring the adsorption strength and catalytic activity.

Several experimental studies have explored how alloy stoichiometry and synthesis environment can affect HER performance. For example, Oliveira et al. [13] synthesized $Fe_xCu_{1-x}$ alloys in aqueous and deep eutectic solvents, finding that Fe-rich alloys exhibited superior catalytic activity when prepared in the latter medium. Similarly, Zhang et al. [14] reported that structural modification, such as N-doped carbon encapsulation in FeNi@NC−NG nanocages, significantly improved the durability of FeNi alloys during electrochemical cycling. Solmaz et al. [15] demonstrated that NiCu coatings on Cu substrates showed substantially enhanced current densities compared to their monometallic counterparts. They attributed this effect to surface porosity and synergistic interactions between Ni and Cu. Moreover, NiCu alloy nanoparticles embedded in carbon frameworks exhibit multifunctional catalytic behavior for OER and HER, maintaining stable performance over extended operation [16].

Together, these findings underscore that bimetallic alloys constitute a versatile and tunable platform for designing efficient HER catalysts. As such, their performance can be systematically optimized by controlling both composition and surface structure, i.e., atomic species exposed to chemical reactions. Beyond alloying advantages, obtaining systems with predictable properties is central in catalyst design. In particular, identify an ideally linear relationship between the alloy ratio and the Gibbs free energy of hydrogen adsorption ($\Delta G_{H^*}$), as it determines the activity of the hydrogen evolution reaction. Such a stoichiometry–activity scaling relation enables rational modulation of catalytic performance by selecting specific atomic ratios. Thus, it provides a direct means to optimize hydrogen binding thermodynamics.

In this context, adjustment of the local electronic environment by stoichiometry control alters the *d*-band center position and charge redistribution between the constituent metals. In turn, this governs the adsorption energetics of hydrogen intermediates. Identifying and understanding bimetallic compounds that follow such linear $\Delta G_{H^*}$-stoichiometry correlations would offer valuable predictive power for the design of catalysts. Thereby, enabling systematic control of the adsorption strength through stoichiometry engineering. This conceptual framework represents an important step toward the development of rational catalysts based on descriptors. Thus, atomic ratio, structure, and property relationships are exploited to optimize adsorption energetics, charge transfer, and catalytic stability under electrochemical conditions [8,17].

Building on these insights, we employ density functional theory (DFT) calculations with van der Waals corrections combined with the computational hydrogen electrode (CHE) model. Within this approach, our objective is to unravel how the atomic ratio and the local atomic environment of the adsorption site modulate $\Delta G_{H^*}$ on the ordered closed-packed non-noble bimetallic substrates. We investigated a series of ordered bimetallic FeNi, FeCu, and NiCu compounds with varying atomic ratios (3:1, 1:1, and 1:3) to establish stoichiometry–activity relationships and identify scaling trends. These transition metals were chosen for their abundance, sustainable synthesis methods, and recovery ability from electronic waste [18,19]. Our analysis reveals that the bimetallic FeNi substrate exhibits a nearly linear dependence between $\Delta G_{H^*}$ and its ratio. This may allow the catalytic activity to be adjusted by varying the atomic ratios of the metallic species that interact with the reaction environment. Although the FeCu and NiCu compounds do not follow a linear trend, specific stoichiometries, namely $FeCu_3$(112) and $NiCu_3$(111), demonstrate favorable HER activity. In all evaluated systems, hydrogen adsorption is energetically favored at hollow sites, where the adsorption energy, the dominant term in $\Delta G_{H^*}$, correlates directly with the identity of atoms within the chemical environment of the local catalytic site.

## 2. Theoretical approach and computational details

### 2.1. Total energy calculations

Our total energy calculations were based on the spin-polarized DFT framework using the semi-local generalized gradient approximation (GGA) as formulated by Perdew–Burke–Ernzerhof (PBE) [20] for the exchange–correlation energy functional, as implemented in the Vienna *Ab initio* Simulation Package (VASP), version 5.4.4 [21,22]. To enhance the description of the long-range van der Waals (vdW) interactions, the semi-empirical vdW D3 correction was applied for all calculations [23]. The interactions between core and valence electrons were modeled employing the projector augmented wave (PAW) method, [24,25]. At the same time, the Kohn–Sham states were expanded using a plane-wave basis set.

We performed stress-tensor calculations to determine the equilibrium lattice parameters of bulk Fe in the body-centered cubic (bcc) structure, as well as bulks Ni and Cu in the face-centered cubic (fcc) structure, employing cutoff energies of 642.014, 714.646, and 834.078 eV, respectively. These values represent twice the maximum recommended cutoff energy for the specified PAW projectors (`ENMAX`), which are required due to the lower convergence of the stress-tensor components as a function of the cutoff energy. For the remaining bulk properties, the cutoff energy was set to 12.5 % higher than the recommended maximum value, resulting in cutoff energies of 361.132, 401.998. and 469.169 eV for Fe, Ni and Cu, respectively. In the case of ordered bimetallic surfaces and hydrogen adsorption, we used a cutoff energy of 401.998 eV for systems containing FeNi, and a cutoff energy of 469.169 eV for the FeCu and NiCu systems.

Integration of the Brillouin zones was performed using equivalent **k**-mesh sampling using the automatic generation process defined with a parameter $R_{\mathbf{k}} = 40$ Å. The same parameter $R_{\mathbf{k}}$ was applied to the evaluated slabs in the *a* and *b* directions, resulting in a **k**-mesh of $9\times9\times1$ for the surfaces (111) and (110) and $9\times5\times1$ for (112). The equilibrium configurations were obtained using a total energy self-consistency criterion of $10^{-6}$ eV and an atomic force convergence criterion of 0.025 eV/Å for each atom. Additional computational details are summarized in the electronic supporting information.

### 2.2. Computational hydrogen electrode model

The hydrogen evolution reaction ($2H^+ + 2e^- \longrightarrow H_2$) is a two-electron transfer process that proceeds through a catalytic reaction intermediate, known as the Volmer step: $H^+ + e^- + * \longrightarrow H^*$, where * denotes the catalytic site [26]. To investigate HER, we calculate the adsorption energy of the reaction intermediate using the following equation:

$$E_{ad}^{H^*} = \frac{1}{n}(E_{tot}^{nH/Slab} - \frac{n}{2}E_{tot}^{H_2} - E_{tot}^{Slab}) , \quad (1)$$

in which $E_{tot}^{nH/Slab}$ is the total energy of the system with adsorbed hydrogen. $E_{tot}^{H_2}$ is the total energy of the $H_2$ molecule in the gas phase, while $E_{tot}^{Slab}$ is the total energy of the clean substrate, and $n$ is the number of adsorbed species H. We assumed a surface coverage of 0.25, considering the most stable adsorption site (hollow fcc or hcp) for all the systems investigated.

Meanwhile, to analyze HER, the proton-coupled electron transfer reaction involved in the mechanism of reaction intermediate formation is evaluated using the computational hydrogen electrode model

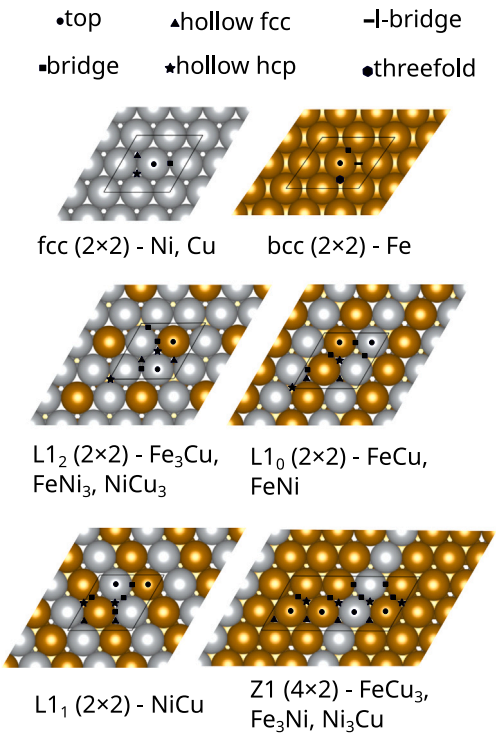


**Fig. 1.** Molecular top-view representations of the Fe, Ni, Cu, FeCu, FeNi, and NiCu substrates are shown. The key high-symmetry H adsorption sites identified on the unary and ordered bimetallic surfaces are indicated. The size of each supercell is outlined with lines.

[27,28]. In this framework, the zero-voltage reference is defined by the reversible hydrogen electrode, where the $\frac{1}{2}H_2 \rightleftharpoons H^+ + e^-$ reaction is considered to be in equilibrium at $U = 0\,V$ at all pH values and temperatures. Consequently, the chemical potential of the proton–electron pair equals half the chemical potential of $H_2$ gas under standard conditions ($\mu_{H^+} + \mu_{e^-} = \frac{1}{2}\mu_{H_2}$). The CHE approach enables the explicit incorporation of U into the free-energy change of each elementary reaction step.

Therefore, the free energies are obtained as follows:

$$G = E_{tot} + E_{ZPE} + \int C_p dT - TS\,, \tag{2}$$

in which $E_{tot}$ is the total electronic energy, $E_{ZPE}$ is the zero-point energy, $\int C_p dT$ represents the contribution of the constant pressure heat capacity, $T$ is the temperature, and $S$ is the contribution of entropy. These contributions are calculated for the gas-phase molecule using the ideal gas approximation and for the adsorbed system using the harmonic limit at a temperature of 298.15 K, as implemented in the Atomic Simulation Environment package [29]. Further details on each contribution used to evaluate the thermodynamic properties are provided elsewhere [29,30].

### 2.3. Atomic structure configurations

*Bulk structures.* The bimetallic alloy substrates under investigation were derived from ordered bulk alloy phases in which the constituent atomic species occupy specific well-defined crystallographic lattice sites in a long-range periodic fashion throughout the material; that is, a non-random occupation of the atomic sites. For example, the binary FeCu compounds show distinct phases of either bcc or fcc structures depending on the atomic fraction involved [31]. In contrast, the fcc phases of $L1_0$ FeNi and $L1_2$ $FeNi_3$ represent the ground states for ordered bimetallic FeNi compound [32]. Consequently, structural prototypes of both bcc and fcc were selected to develop ordered bimetallic FeNi, FeCu, and NiCu substrates with varied atomic ratios: 3:1 and 1:1. The ordered bcc-type prototypes chosen include $D0_3$ ($AlFe_3$, $Fm\bar{3}m$ space group) and $B2$ (CsCl, $Pm\bar{3}m$ space group), while the fcc-type prototypes encompass $L1_0$ (AuCu, $P4/mmm$ space group), $L1_2$ ($AuCu_3$, $Pm\bar{3}m$ space group), $L1_1$ (CuPt, $R\bar{3}m$ space group) [33], and $Z1$ ((001) $Fe_3$/Ni superlattice) [34]. Furthermore, PBE+D3 computations revealed that, across all examined ordered bimetallic structures, the fcc-type structures represent the lowest-energy configurations.

*Surface terminations.* The (111) surface is widely recognized as the most stable termination for fcc metals due to its high atomic packing density and correspondingly low surface energy [35]. In this work, we focus on ordered bimetallic substrates designed so that bulk stoichiometry is preserved in all atomic layers. This constraint naturally leads to the selection of closed-packed facets, most commonly the (111) plane, because they allow the intrinsic bimetallic ratio to be faithfully exposed on the surface. Each slab model consists of five atomic layers and includes a vacuum region of 15 Å to avoid spurious interactions among the slabs. In addition to the unary references Ni(111) and Cu(111), the bimetallic surfaces considered in this study comprise: $L1_2$ $Fe_3Cu(111)$, $L1_0$ FeCu(111), $Z1$ $FeCu_3(112)$, $Z1$ $Fe_3Ni(112)$, $L1_0$ FeNi(111), $L1_2$ $FeNi_3(111)$, $Z1$ $Ni_3Cu(112)$, $L1_1$ NiCu(110), and $L1_2$ $NiCu_3(111)$. Among these, the only non-close-packed termination is the Fe(110) surface, which is nevertheless included because it represents the thermodynamically most stable facet for bcc iron [36]. To ensure consistency in lateral dimensions, which will affect the adsorbate-adsorbate interactions, all (111) and (110) ordered bimetallic surfaces were constructed as $2\times2$ supercells, while the termination (112) required a larger $4\times2$ supercell due to their lower symmetry. This unified modeling strategy enables direct and controlled comparison of the adsorption behavior across different bimetallic substrates while physically preserving meaningful surface stoichiometries.

*Hydrogen adsorption on substrates.* We performed H adsorption on both sides of the slab to mitigate dipole moment effects in supercells, since each atomic layer has the same atomic fraction, resulting in an equal electrostatic potential along the $z$-direction. The surface coverage of the 0.25 monolayer was evaluated for all systems. For the $4\times2$ supercell, an additional H atom was adsorbed on the substrate. Fig. 1 presents the surface sites assessed for adsorption. Initially, adsorption was assessed using a fully constrained substrate, with relaxation permitted only for the H atom due to the significant mass difference between hydrogen and transition metal atoms and also the large mobility on (111) surfaces [37]. Subsequently, different low-energy adsorption site configurations within a range of 5 meV/atom were identified for relaxation, this time constraining only the middle atomic layer of the substrate. Ultimately, to assess the thermodynamic properties related to HER for the lowest energy systems, vibrational calculations were performed that allow for finite displacements of 0.015 Å exclusively for the adsorbates. Furthermore, the gas-phase $H_2$ molecule was relaxed via $\Gamma$-point calculations within a cubic box of 20 Å. Additional details on the theoretical approach and computational framework are reported in the electronic supporting information.

## 3. Results and discussion

To understand the HER on the evaluated substrates, we structured our discussions around energetic properties. First, we focus on hydrogen (H) adsorption, followed by thermodynamic contributions and application of the CHE model. Furthermore, we explain the energetic behavior by analyzing the electronic properties, which deepens our comprehension of these systems.

**Table 1**
Hydrogen adsorption site description, adsorption energy ($E_{ad}^{H^*}$), and average distance between the adsorbed H and surface chemical species at the adsorption site ($d_{av}^{H-TM}$), where TM = Fe, Ni, Cu, and the vertical distance between the adsorbate and plane composed by the adsorption site ($d_{av}^{H-Surf}$). All distances are given in angstroms (Å).

| H/Substrate | Adsorption site | $E_{ad}^{H^*}$ (eV) | $d_{av}^{H-Fe}$ | $d_{av}^{H-Ni}$ | $d_{av}^{H-Cu}$ | $d_{av}^{H-Surf}$ |
|---|---|---|---|---|---|---|
| Fe(110) | FeFeFe | −0.84 | 1.78 | | | 0.95 |
| Ni(111) | NiNiNi | −0.66 | | 1.69 | | 0.91 |
| Cu(111) | CuCuCu | −0.34 | | | 1.73 | 0.91 |
| $Fe_3Cu$(111) | FeFeFe | −0.88 | 1.77 | | | 1.02 |
| FeCu(111) | FeFeCu | −0.71 | 1.76 | | 1.79 | 1.01 |
| $FeCu_3$(112) | FeFeCu | −0.69 | 1.72 | | 1.83 | 0.97 |
| $Fe_3Ni$(112) | FeFeFe | −0.83 | 1.75 | | | 0.99 |
| FeNi(111) | FeNiNi | −0.75 | 1.79 | 1.70 | | 0.95 |
| $FeNi_3$(111) | NiNiNi | −0.68 | | 1.70 | | 0.91 |
| $Ni_3Cu$(112) | NiNiNi | −0.71 | | 1.68 | | 0.89 |
| NiCu(110) | NiNiCu | −0.74 | | 1.66 | 1.80 | 0.91 |
| $NiCu_3$(111) | NiCuCu | −0.60 | | 1.62 | 1.75 | 0.90 |

### 3.1. Hydrogen adsorption on non-noble metallic substrates

As discussed in the previous sections, the Volmer step plays a central role in the hydrogen evolution reaction, as it governs the formation of the key reaction intermediate, H*. Consequently, the free energy of H adsorption is widely considered the primary activity descriptor that influences the overall reaction rate [2]. Because the adsorption energy represents a substantial fraction of the energetic cost associated with generating H*, its accurate determination is essential to reliably assess catalytic performance. In this work, the adsorption energy is calculated with respect to the $H_2$ molecule, following Eq. (1). The resulting adsorption energies, along with the characterization of the most stable adsorption sites and key geometric parameters, are summarized in Table 1. To maintain clarity in the nomenclature, we adopt the general designation *AB* to represent the ordered bimetallic substrate family that includes the stoichiometries $A_3B$, *AB*, and $AB_3$. However, for each specific substrate, the exact chemical composition and corresponding crystallographic orientation (Miller index) are explicitly reported.

For unary substrates, the absolute adsorption energies at the most stable surface sites exhibit the following trend Fe > Ni > Cu, which is consistent with previous PBE+D3 calculations [38]. The hollow site consistently emerges as the most stable site for H binding. Each hollow site comprises a threefold coordinated configuration, which may encompass atoms of a singular element or a composite of a 2:1 atomic ratio. In the case of bimetallic FeNi and FeCu, the binding energy is influenced by synergistic effects, representing the proportional contribution of each chemical species at the catalytic site. This behavior is absent in NiCu compounds, wherein the inclusion of at least one Ni atom within the hollow site causes the adsorption energy to approximate that of the pristine Ni(111) substrate. In addition, the pristine Cu(111) exhibits the weakest H adsorption energy, reflecting a weak H−Cu interaction. This weak interaction is also present in bimetallic substrates based on Cu, which affects hydrogen adsorption. Specifically, on substrates where the Cu atomic ratio is predominant, this process favors hollow sites composed of mixed elements over unary Cu, thus increasing the adsorption energy. In contrast, for substrates where Fe or Ni has the highest atomic ratio, adsorption of H will occur in hollow sites consisting exclusively of Fe or Ni, respectively. In these cases, the adsorption energies will be close to those of their pristine substrate counterparts.

In Table 1, we also show the average distance between hydrogen and exposed atoms at the surface site, as well as the vertical distance between adsorbed H and the plane composed of hollow atoms, considering only the middle atomic layer of the frozen substrate. The average distances follow the trend $d_{av}^{H-Ni} < d_{av}^{H-Cu} < d_{av}^{H-Fe}$. The vertical distance agrees with calculations from the previous literature [39–41]. Besides, $d_{av}^{H-Fe}$, $d_{av}^{H-Ni}$, and $d_{av}^{H-Cu}$ approach the values observed on the corresponding unary substrates as the atomic fraction increases. The stronger the interaction H−TM on the unary metal substrate, the closer H will adsorb to that metal in ordered bimetallic systems, except for FeNi(111).

The surface sites incorporating Fe demonstrate the greatest vertical separations between H and the atomic plane containing the adsorption site, with these separations decreasing as the atomic fraction of Fe decreases. Atoms of Fe possess the largest atomic radius among the atomic species considered, influencing surface corrugation. Additionally, Fe atoms at the surface site exhibit a slightly more positive charge relative to their unary counterparts. Bimetallic substrates based on NiCu exhibit vertical distances similar to those found in unary substrates, and both chemical species have a similar atomic radius.

### 3.2. Effect of bimetallic ratio on HER activity

In the preceding section, we examined the energetic characteristics of ordered bimetallic substrates upon H adsorption. The Gibbs free energy of the reaction intermediate ($\Delta G_{H^*}$), in relation to the reactant at equilibrium potential within the CHE model, is one of the crucial parameters for evaluating catalytic activity [42,43].

The thermodynamic properties related to the hydrogen evolution reaction (HER) are presented in Table 2. Entropic contributions exhibit uniform variation across all cases, as noted in 0.20 eV. The variation in zero point energy influences the reaction enthalpy by an amount ranging from 0.04 to 0.06 eV. In turn, the variation in the heat capacity contributes approximately −0.04 eV. Consequently, given a consistent zero point energy and entropic contribution, the differences observed in the HER activity among the substrates are primarily attributed to the inherent electronic characteristics of each system. In other words, the fluctuations in free energy from one system to another are largely dependent on the binding energy of each system when the CHE method is employed.

In Fig. 2, we show the free energy diagrams for HER in the ordered bimetallic substrates. Depending on the Cu atomic fraction, the catalytic HER activity can be enhanced. At an atomic fraction of 25 %, the strength of the adsorption of H increases slightly for FeCu and NiCu systems compared to Fe(110) and Ni(111), respectively, resulting in a lower HER activity. At 50 % of Cu, $\Delta G_{H^*}$ for FeCu increases, while it decreases for NiCu. For higher concentrations of Cu, the $\Delta G_{H^*}$ increases for all systems, thus increasing the HER activity. The state-of-the-art Pt catalyst exhibits on the (111) surface a $\Delta G_{H^*} = -0.18$ eV (RPBE) and −0.25 eV (PBE) [44,45]. Among the non-noble ordered bimetallic compounds, $NiCu_3$(111) is the most active for HER, as described by the thermodynamic descriptor $\Delta G_{H^*} = -0.39$ eV.

Santos et al. [46] showed that incorporation of Cu into CoMo alloys improved the catalytic activity for HER by lowering the overpotential required to reach a current density of $-10\ mA\ cm^{-2}$ from 156 mV (CoMo) to 119 mV (CoMoCu). This behavior was also reported for Cu-doped cobalt pyrite ($CoS_2$), in which the dopants weaken the bond strength of H−S, thus enhancing HER activity [47]. From our results, we can see that high Cu loading usually helps increase $\Delta G_{H^*}$, so lower overpotentials would be required for HER. In addition, the unary substrate Cu presents the highest $\Delta G_{H^*}$.

PBE+D3 free energies for the adsorption of H on Cu(111) approximate zero; however, it is well established that Cu demonstrates weak adsorption properties and manifests low catalytic activity for HER [48]. Moreover, PBE+D3 tends to overestimate adsorption energies for various adsorbates [49,50]. In addition, close to and at the Fermi level, Cu(111), dominated by *d*-states, has a negligible density of states. Consequently, the overlap with the hydrogen *s*-orbital falls below the distance typically required for electron transfer [45,51]. Our calculations were performed without a solvent environment. Implicit models offer an affordable way to include these effects; however, they can lead to an inaccurate description of the interfacial electric field, resulting

**Table 2**
Thermodynamic data of H* adsorption on ordered bimetallic substrates considering a coverage of 0.25. The data correspond to 1 bar, pH = 0 at 298.15 K.

| Substrate | $E_{ad}^{H^*}$ (eV) | $\Delta G_{H^*}$ (eV) | $\Delta(\int C_p dT)$ (eV) | $-T\Delta S_{H^*}$ (eV) | $\Delta ZPE_{H^*}$ (eV) |
|---|---|---|---|---|---|
| Fe(110) | −0.84 | −0.64 | −0.04 | 0.20 | 0.04 |
| Ni(111) | −0.66 | −0.45 | −0.04 | 0.20 | 0.05 |
| Cu(111) | −0.34 | −0.14 | −0.04 | 0.20 | 0.04 |
| $Fe_3Cu(111)$ | −0.88 | −0.67 | −0.04 | 0.20 | 0.05 |
| FeCu(111) | −0.71 | −0.51 | −0.04 | 0.20 | 0.04 |
| $FeCu_3(112)$ | −0.69 | −0.48 | −0.04 | 0.20 | 0.05 |
| $Fe_3Ni(112)$ | −0.83 | −0.61 | −0.04 | 0.20 | 0.06 |
| FeNi(111) | −0.75 | −0.54 | −0.04 | 0.20 | 0.05 |
| $FeNi_3(111)$ | −0.68 | −0.47 | −0.04 | 0.20 | 0.05 |
| $Ni_3Cu(112)$ | −0.71 | −0.49 | −0.04 | 0.20 | 0.06 |
| NiCu(110) | −0.74 | −0.53 | −0.04 | 0.20 | 0.05 |
| $NiCu_3(111)$ | −0.60 | −0.39 | −0.04 | 0.20 | 0.05 |

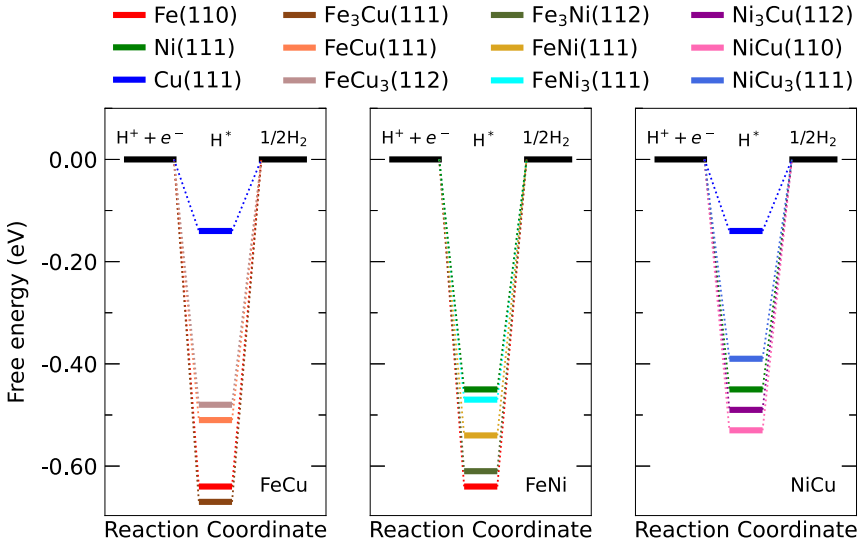


**Fig. 2.** Free energy diagram for HER on ordered bimetallic substrates with 0.25 coverage.

in erroneous reaction energies [52]. Additionally, implicit models for a series of reaction intermediates do not show improvement when compared with vacuum calculations [53]. On the other hand, explicit solvent modeling is computationally demanding and requires further investigation.

Fig. 3 illustrates the correlation between $\Delta G_{H^*}$ and the substrate stoichiometry. The increase in $\Delta G_{H^*}$ with increasing atomic fraction $x$ indicates the incorporation of a transition metal that interacts more weakly with H. The FeNi substrates demonstrate a pronounced linear correlation between $\Delta G_{H^*}$ and atomic ratio, which is an important behavior in the development of low-cost electrocatalysts. The $\Delta G_{H^*}$ values of the unary metals delineate the energetic boundaries of the FeNi compounds, with Fe and Ni representing the lower and upper limits, respectively. This behavior is attributed to the local atomic environment of the catalytic site. In the FeNi substrates, the chemical environment of the catalytic site progressively changes from Fe to Ni, as indicated in Table 1. However, this transformation is not evident in bimetallic compounds containing Cu, as a catalytic site constituted exclusively of Cu is less energetically favorable for adsorption. Consequently, HER activity, when based on the descriptor $\Delta G_{H^*}$, can be modulated first by chemical composition; secondly, and invariably, by increasing the atomic fraction of a transition metal whose unary form interacts less strongly with H, thus enhancing HER activity.

### 3.3. Electronic origins of HER activity in ordered bimetallic alloys

To gain deeper insights into the influence of electronic properties on HER performance, we studied the local density of states (LDOS), $d$-band center, effective charges computed using the density-derived electrostatic and chemical (DDEC) method [54,55], and the electronic density difference (EDD) of the evaluated ordered bimetallic substrates.

Fig. 4 shows the LDOS of the catalytic site for each substrate before hydrogen adsorption and the element-weighted $d$-band center. We evaluated adsorption trends using the $d$-band model developed by Hammer and Nørskov [56]. According to this model, the closer the center of the $d$-band lies to the Fermi level, the more likely the catalyst will exhibit strong adsorption activity [57]. The adsorption energy follows the trend of the $d$-band center. From Fe to Cu, the number of $d$-electrons increases, filling the $d$-states and causing a shift of the band center to lower energy, which weakens the reactivity. The mixture of transition metals alters the electronic structure, and the presence of different chemical species at the adsorption site modifies both the filling of the $d$-band and the bandwidth. In Fig. 5, we can see that there is a good correlation ($R^2 = 0.814$) between the H adsorption energy and the weighted $d$-band center of the adsorption site. As the fraction of the transition metal whose unary counterpart interacts least with hydrogen increases on the substrate, the element-weighted $d$-band center shifts farther from the Fermi level. Thus, we indicate that the atomic environment of the catalytic site helps modulate the strength of hydrogen adsorption. Therefore, the $d$-band center is a valuable descriptor in the search for an efficient catalyst for HER in the case of ordered bimetallic systems.

In Fig. 6, we depict the LDOS associated with the adsorbed catalytic sites, which encompasses the $d$-states of the surface atoms and the electronic states of the hydrogen adsorbate. The states originating from H demonstrate a significant intensity within the energy interval of −8 to

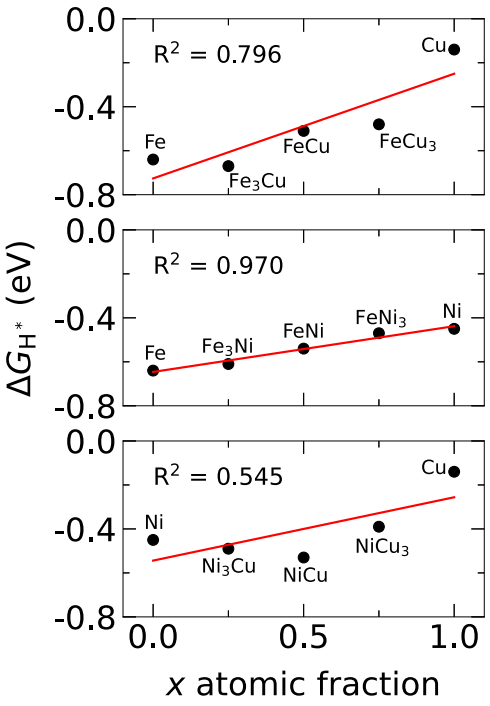


**Fig. 3.** Correlation analysis between different stoichiometries, indicated by $x$, and $\Delta G_{H^*}$ for $A_{(1-x)}B_x$.

−5 eV, where they hybridize with the $d$ orbitals of the transition metals, which signals considerable electronic delocalization. The presence of Fe atoms in the catalytic site increases the spin polarization of the states H, indicative of the magnetic properties inherent in environments rich in Fe. Upon adsorption of H, the $d$-band center, weighted by the local chemical environment, experiences a shift towards lower energies relative to the Fermi level. This shift implies a reduction in the adsorption strength for successive H species, which is in agreement with the notion of repulsive lateral interactions as the surface coverage increases. These alterations in electronic structure underscore the dependence of hydrogen-binding energetics on the local chemical stoichiometry in ordered bimetallic surfaces.

DDEC charges were determined for all systems before and after H adsorption. The effective charge on the outermost surface atoms of the unary substrates is $-0.01\,e$. The effective charges in the catalysts change depending on the chemical composition and ratio due to charge redistribution. For example, FeCu substrates exhibit minor changes compared to unary substrates, with the highest variation approximately $0.03\,e$. In contrast, the FeNi and NiCu bimetallic compounds show more pronounced changes in the charges of the exposed atoms, with positively and negatively charged atoms present. The atomic fraction can also intensify the charge redistribution, as observed in FeNi and NiCu substrates, see Figures S-36 to S-38 in the SI file. The Cu atoms in the bimetallic compounds are positively charged, indicating charge transfer to the other TM that is more negatively charged.

Adsorption of H occurs at the hollow site, where its first neighbors exhibited a negative charge before adsorption, with Fe or Ni as the closest neighbor in ordered bimetallic substrates. Therefore, a charge transfer occurs from the substrate to the adsorbed H, resulting in a negatively charged adsorbate. The charge on the adsorbed hydrogen ranges from −0.02 to $-0.09\,e$. In particular, systems with a higher concentration of Cu show a higher substrate-to-hydrogen charge transfer. Inspecting Fig. 6, we can see an overlapping increase between the Cu $d$-band states and the hydrogen states around −6 eV as the concentration of Cu increases, helping to explain the charge transfer behavior.

We performed an EDD analysis to confirm the presence of the charge transfer mechanism, using the following equation:

$$\Delta\rho(\mathbf{r}) = \rho^{n\mathrm{H/Slab}}(\mathbf{r}) - \rho^{n\mathrm{H}}(\mathbf{r}) - \rho^{\mathrm{Slab}}(\mathbf{r})\ , \tag{3}$$

where $\rho^{n\mathrm{H/Slab}}(\mathbf{r})$, $\rho^{n\mathrm{H}}(\mathbf{r})$, and $\rho^{\mathrm{Slab}}(\mathbf{r})$ represent the electronic densities of the total system, the isolated H atom in its adsorbed position, and the frozen substrate, respectively. In Fig. 7, we show the EDD for all systems studied. The charge analysis allows us to evaluate the charge transfer mechanism. In all cases, the charge density depletes from the atoms that compose the local catalytic site and accumulates on the adsorbed hydrogen. All are consistent with their final charges obtained, with positive values for TMs and negative values for H.

As we had discussed, there is an energetic pattern for the adsorption of H, where TM that strongly bonds to H in its unary form will also strongly bond to H on surfaces with higher concentrations of this TM. In contrast, adding another TM atom that binds to H more weakly in its unary form will weaken the adsorption energy. That is, the presence of low-energy binding species can modulate the adsorption energy, and FeNi ordered substrates are an example.

However, this trend does not apply to NiCu. The 1:1 atomic fraction exhibits the highest adsorption energy (in absolute value) among the NiCu bimetallic substrates. In this case (NiCu(110)), the induced electron density redistribution can extend to the middle layer of the substrate, while in Ni(111) and $Ni_3Cu$(112), the redistribution is observed in the second layer. This characteristic may contribute to the highest H-substrate interaction for NiCu(110). A similar behavior occurs in the adsorption of rare gases in Pd(111), where the adsorption energy increases from He to Xe, and the electronic redistribution observed in the EDD becomes more pronounced in the inner Pd atomic layers in the same order as the adsorption energy [58].

## 4. Future of Fe, Ni and Cu alloys for HER

In general, bimetallic catalysts are designed to benefit from the specific properties of their monometallic counterparts. This is known as synergistic effects, in which the properties of each metal are generally combined to enhance the catalytic activity of the final material [59]. This effect is commonly attributed to modifications in the electronic structure and geometric configuration of the active material [60]. Theoretical calculations contribute to a deeper understanding of these interactions, shedding light on the nature of these effects at the atomic level. Furthermore, it helps rationalize the experimentally observed catalytic descriptors and even find optimized atomic fractions [61,62].

The synergistic interaction between Fe and other transition metals, such as Ni and Cu, is a recurring theme in the design of HER catalysts [63]. The alloying of Fe with Ni or Cu has been used as a strategy to modulate the electronic structure of the final system. Thus, optimizing the energy of hydrogen adsorption and improving catalyst activity [64]. For example, although Cu exhibits weak proton adsorption, it can improve conductivity, stability, and resistance to corrosion of the prepared material, which are critical parameters for catalytic performance in electrochemical reactions [65].

On the other hand, Fe are known to adsorb and activate protons effectively [66]. When Fe and Cu are combined, a synergistic interaction results in a catalyst that balances activity, stability, and conductivity, outperforming individual metals [67]. For example, for substrates based on FeCu, we verify an improvement in the energy of proton adsorption at a low Fe content compared to Cu(111). This is a result of the better adsorption of the H to Fe sites. From the free energy diagram, we see that $FeCu_3$ presents a closer to the optimal adsorption ($\Delta G_{H^*} \approx 0$ eV), indicating a possibly better activity for HER.

In contrast, at a low Cu content, a stronger H adsorption was found ($Fe_3Cu$(111)) compared to Fe(110). Here, the effect of Fe being exposed to hydrogen is combined with a charge transfer from Cu to its surroundings, which makes the Fe sites slightly more reactive. In turn, this increases the hydrogen adsorption energy; consequently, its

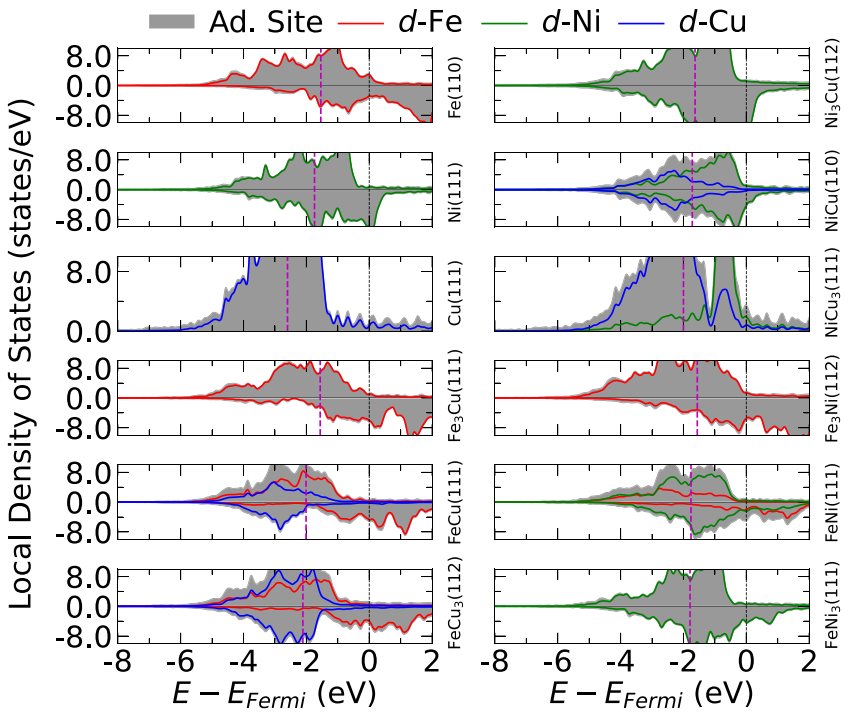


**Fig. 4.** LDOS of the atoms that constitute the most stable adsorption site before the H adsorption for each evaluated substrate. The magenta dashed lines represent the weighted *d*-band center with respect to the chemical environment of the catalytic site.

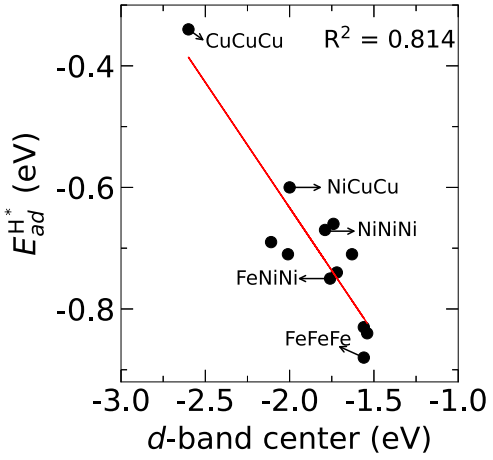


**Fig. 5.** Correlation between the hydrogen adsorption energy and the catalytic site chemical environment weighted *d*-band center. The description of each site is in Table 1.

$\Delta G_{H^*}$ is far from optimal considering HER applications. In addition, Fe can also tune the electronic properties of Ni [68]. According to our models, the overall catalytic performance of FeNi can be changed by its stoichiometry. For example, the FeNi(111) substrate exhibited a hydrogen adsorption free energy of −0.54 eV, which is an intermediate value compared to unary Fe(110) (−0.64 eV) and Ni(111) (−0.45 eV).

The complementary properties of Ni and Cu also show great advantages for HER [59]. Ni is well-known for its intrinsic catalytic activity for the release of $H_2$ [69]. However, it suffers from moderate conductivity and limited long-term stability [70]. In this sense, Cu can contribute to improving the structural stability and corrosion resistance of the material. In addition, the interaction Cu–Ni contributes to increasing the catalytic site activity. Thus, increasing the hydrogen adsorption energy. As discussed, at higher Cu loading, the NiCu bimetallic substrate will be more Cu(111)-like, decreasing the hydrogen adsorption energy. Subsequently, our calculations indicated that among the stoichiometries of the surfaces evaluated, $NiCu_3$ exhibits the optimal free energy for HER. In this regard, Ahsan and coworkers described the synthesis of $NiCu_3$ nanoparticles that exhibited distinct activity not only for HER but also for oxygen reduction and oxygen evolution reactions, highlighting the relevance of this ratio [16].

Metal alloys as catalysts for WE, particularly transition metal-based catalysts, are promising due to their abundance and possible integration with sustainable synthesis methods with a low carbon footprint [18]. For example, metals such as Fe, Ni, and Cu can be recovered from secondary resources, such as nonfunctional electronic devices, commonly called electronic waste [71]. The process of using recycled metals to prepare catalyst materials supports the principles of a circular economy by reducing both waste generation and greenhouse gas emissions [19].

In addition, alloy catalysts can be prepared by electrochemical synthesis, which is generally fast, inexpensive, and easy to conduct in one step under ambient pressure and low temperatures [72]. Electrodeposition enables precise control over the substrate material and geometry, as well as the electrolyte composition, making it highly adaptable for catalyst design [73]. The literature has reported that the choice of substrate for catalyst electrodeposition plays a critical role in determining the nucleation behavior, morphology, and ultimately the distribution and nature of active sites [74].

From a theoretical perspective, it is also known that the substrate can influence the surface energy landscape and the initial growth orientation of the deposited material. It can affect structural properties such as crystallinity, grain boundaries, and defect density. In addition to affecting the growth of the physical alloy, the substrate can also modulate its electronic structure and active surface sites through interfacial interactions [75]. In this sense, it is essential to note that, beyond the application of a theoretical framework to analyze possible substrate ratios, there is still scope to investigate the impact of substrate-induced effects, such as charge redistribution or strain, on the catalytic behavior. Ultimately, integrating computational and experimental approaches is essential to plan transition-metal-based materials as cost-effective and efficient WE catalysts, paving the way for their application in sustainable hydrogen production.

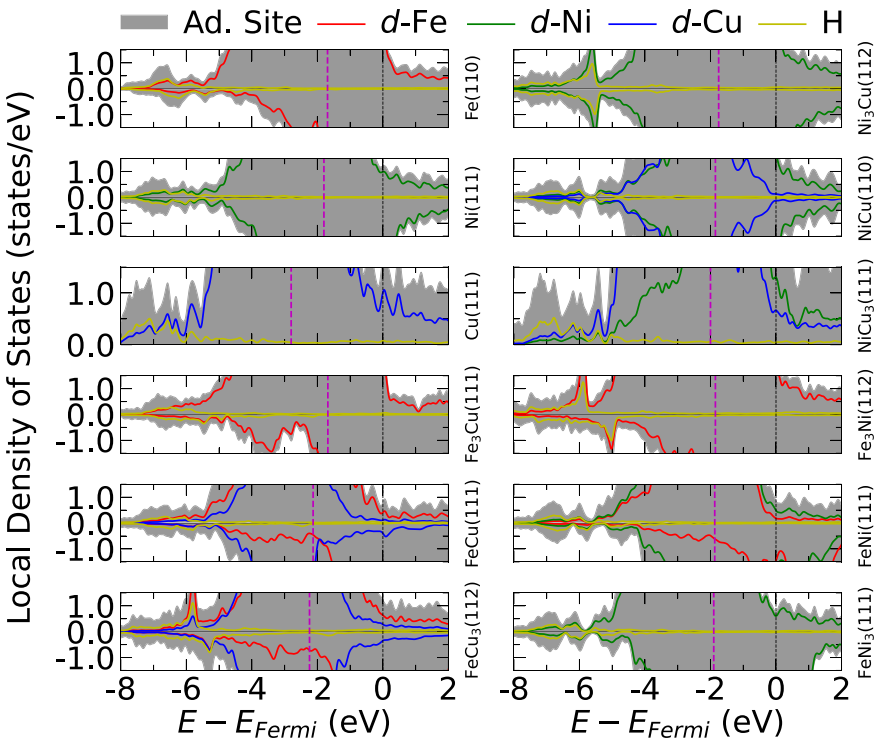


**Fig. 6.** LDOS of the catalytic site for each substrate after the H adsorption. The magenta dashed lines represent the weighted $d$-band center with respect to the catalytic site chemical environment.

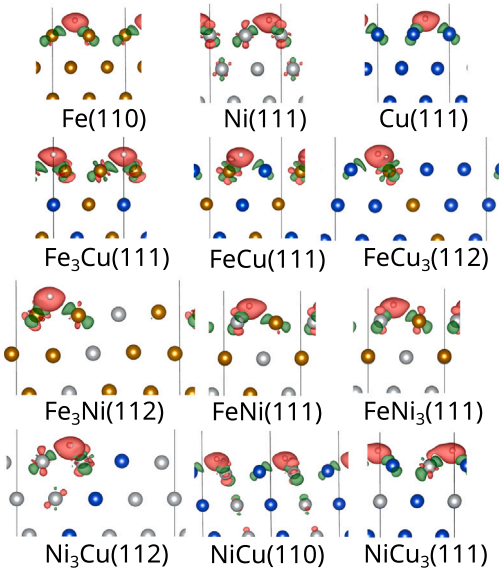


**Fig. 7.** Electron density difference plots using isosurfaces with $0.004\,\mathrm{bohr}^{-3}$ value for H adsorption on evaluated substrates. The red region represents charge accumulation, and the green region represents charge depletion.

## 5. Conclusions

In this work, we employ DFT calculations using the PBE functional with D3 van der Waals corrections, combined with the computational hydrogen electrode model, to investigate the stoichiometry dependence of the hydrogen evolution reaction on closed-packed ordered bimetallic surfaces. Our main goal was to delineate the role of substrate stoichiometry variations and atomic-scale structure modulating the hydrogen adsorption Gibbs free energy and to identify descriptors that guide the rational design of efficient, non-noble transition-metal catalysts. We examine FeNi, FeCu, and NiCu ordered bimetallic catalysts with different atomic ratios (3:1, 1:1, and 1:3) to establish stoichiometry-activity relationships and to understand how the mixture influences local electronic environments and catalytic performance.

Our results reveal that alloying can tune the hydrogen adsorption energetics by modifying the local charge distribution and the $d$-band electronic structure of the catalytic site. The FeNi compounds, in particular, exhibit a nearly linear dependence between $\Delta G_{H^*}$ and substrate stoichiometry, suggesting that catalytic activity can be predictably controlled by adjusting the fraction of the constituent metals. This linear scaling behavior provides an alternative to designing catalysts with optimal adsorption energetics, approaching the thermoneutral condition ($\Delta G_{H^*} \approx 0\,\mathrm{eV}$).

In contrast, FeCu and NiCu deviate from this linear trend due to variations in the chemical environment of the catalytic site. Nevertheless, the specific ordered configurations $FeCu_3(112)$ and $NiCu_3(111)$ still exhibit favorable $\Delta G_{H^*}$ values, indicating that the targeted stoichiometry adjustment can lead to high activity even in systems without global linear behavior. Electronic analyses further demonstrate that hydrogen adsorption occurs preferentially at hollow sites, where charge transfer proceeds from the substrate to the adsorbate. The adsorption energy, dominating the Gibbs free energy contribution, correlates with the chemical identity of the atoms within the hollow sites and the position of the element-weighted $d$-band center relative to the Fermi level.

Overall, this study establishes a clear connection between substrate stoichiometry, electronic structure, and hydrogen adsorption energetics in ordered close-packed bimetallic substrates. The demonstrated ability to modulate $\Delta G_{H^*}$ through controlled alloying can encourage the rational design of non-noble transition-metal catalysts for water electrolysis. These insights highlight the importance of integrating electronic descriptors and chemical control in the search for cost-effective, sustainable, and high-performance HER electrocatalysts.

## CRediT authorship contribution statement

**Pedro Ivo R. Moraes:** Writing – review & editing, Writing – original draft, Methodology, Investigation, Formal analysis, Data curation, Conceptualization. **Rafael L.H. Freire:** Writing – review & editing, Writing – original draft, Methodology, Formal analysis, Data curation. **Marina Medina:** Writing – review & editing, Writing – original draft, Conceptualization. **Juliana F. Brito:** Writing – review & editing, Writing – original draft. **Lucia H. Mascaro:** Writing – review & editing, Writing – original draft. **Juarez L.F. Da Silva:** Writing – review & editing, Writing – original draft, Supervision, Resources, Project administration, Methodology, Data curation, Conceptualization.

## Data and software availability

The authors declare no competing financial interest. As mentioned, all DFT calculations were performed using the Vienna *Ab initio* Simulation Package, which can be used under a non-free academic license. Additional details can be obtained from the link https://www.vasp.at/. Additional details are provided in the electronic supporting information, while additional crude data can be obtained directly from the authors upon reasonable request.

## Declaration of competing interest

The authors declare the following financial interests/personal relationships which may be considered as potential competing interests: Juarez L. F. Da Silva reports financial support was provided by University of Sao Paulo Campus of Sao Carlos. Juarez L. F. Da Silva reports a relationship with University of São Paulo that includes: employment. If there are other authors, they declare that they have no known competing financial interests or personal relationships that could have appeared to influence the work reported in this paper.

## Acknowledgments

The authors gratefully acknowledge support from FAPESP (São Paulo Research Foundation), Brazil and Shell, United States, grant Numbers 2017/11631-2 and 2018/21401-7, and the strategic importance of the support given by ANP (Brazil's National Oil, Natural Gas and Biofuels Agency) through the R&D levy regulation. P. I. R. Moraes and M. Medina acknowledge the financial support (Post-doctoral fellowship) from FAPESP, Brazil, grant Numbers 2023/12824-0 and 2023/14228-5. J. F. Brito acknowledges FAPESP, Brazil 2023/10027-5, Instituto Serrapilheira, Brazil - Grant number Serra–2211–41925, and CNPq (Conselho Nacional de Desenvolvimento Científico e Tecnológico), Brazil grant numbers 406156/2022-0, 180111/2023-0. The authors also thank the infrastructure provided to our computer cluster by the Department of Information Technology – Campus São Carlos. The research was developed with the help of HPC resources provided by the Information Technology Superintendence of the University of São Paulo. We acknowledge the use of advanced language models for their assistance in English grammar review.

## Appendix A. Supplementary data

The data employed for the Figures, as well as complementary analyses and additional technical details, are reported within the supplementary material (SM).

Supplementary material related to this article can be found online at https://doi.org/10.1016/j.ijhydene.2026.153692.

## References

[1] Chu S, Majumdar A. Opportunities and challenges for a sustainable energy future. Nature 2012;488:294–303. http://dx.doi.org/10.1038/nature11475.
[2] Seh ZW, Kibsgaard J, Dickens CF, Chorkendorff I, Nørskov JK, Jaramillo TF. Combining theory and experiment in electrocatalysis: Insights into materials design. Science 2017;355. http://dx.doi.org/10.1126/science.aad4998.
[3] Singh R, Singh M, Gautam S. Hydrogen economy, energy, and liquid organic carriers for its mobility. Mater Today:. Proc 2021;46:5420–7. http://dx.doi.org/10.1016/j.matpr.2020.09.065.
[4] Horn R, Schlögl R. Methane activation by heterogeneous catalysis. Catal Lett 2015;145:23–39. http://dx.doi.org/10.1007/s10562-014-1417-z.
[5] Medina M, Brunca da Silva A, Xia L, Jiang W, Glüsen A, Ribeiro C, Mascaro LH. Tailoring NiFeS microstructure through electrodeposition for high-performance anion exchange membrane water electrolysis. J Power Sources 2025;657:238128. http://dx.doi.org/10.1016/j.jpowsour.2025.238128.
[6] dos Santos KG, Eckert CT, De Rossi E, Bariccatti RA, Frigo EP, Lindino CA, Alves HJ. Hydrogen production in the electrolysis of water in Brazil, a review. Renew Sustain Energy Rev 2017;68:563–71. http://dx.doi.org/10.1016/j.rser.2016.09.128.
[7] Conway BE, Tilak BV. Interfacial processes involving electrocatalytic evolution and oxidation of $H_2$, and the role of chemisorbed H. Electrochim Acta 2002;47:3571–94. http://dx.doi.org/10.1016/S0013-4686(02)00329-8.
[8] Jin D, Qiao F, Chu H, Xie Y. Progress in electrocatalytic hydrogen evolution of transition metal alloys: Synthesis, structure, and mechanism analysis. Nanoscale 2023;15:7202–26. http://dx.doi.org/10.1039/D3NR00514C.
[9] Wang J, Xin S, Xiao Y, Zhang Z, Li Z, Zhang W, Li C, Bao R, Peng J, Yi J, Chou S. Manipulating the water dissociation electrocatalytic sites of bimetallic nickel-based alloys for highly efficient alkaline hydrogen evolution. Angew Chem Int Ed 2022;61:e202202518. http://dx.doi.org/10.1002/anie.202202518.
[10] Shen S, Li Q, Zhang H, Yang D, Gong J, Gu L, Gao T, Zhong W. Negative-valent platinum stabilized by Pt–Ni electron bridges on oxygen-deficient NiFe-LDH for enhanced electrocatalytic hydrogen evolution. Adv Mater 2025;37:2500595. http://dx.doi.org/10.1002/adma.202500595.
[11] Wang Y, Zhang J, Wang X, Meng W, Ren D, Tong B, Han C. Bimetal-organic framework-derived nanorod-like $Fe_xNi_{1-x}$@C, P composites for electrochemical hydrogen evolution. J Alloys Compd 2023;931:167511. http://dx.doi.org/10.1016/j.jallcom.2022.167511.
[12] Zhou B, Gao R, Zou J-J, Yang H. Surface design strategy of catalysts for water electrolysis. Small 2022;18:2202336. http://dx.doi.org/10.1002/smll.202202336.
[13] de Oliveira RC, Sousa NG, da Silva LTV, do Nascimento RF, Mascaro LH, Casciano PNS, Oliveira TMBF, Lima-Neto Pd, Correia AN. The role of $Fe_xCu_{1-x}$ electrodeposits from a deep eutectic solvent in promoting the hydrogen evolution reaction. Int J Hydrog Energy 2024;93:346–54. http://dx.doi.org/10.1016/j.ijhydene.2024.10.311.
[14] Zhang X, Li C, Si T, Lei H, Wei C, Sun Y, Zhan T, Liu Q, Guo J. FeNi cubic Cage@N-Doped carbon coupled with N-doped graphene toward efficient electrochemical water oxidation. ACS Sustain Chem Eng 2018;6:8266–73. http://dx.doi.org/10.1021/acssuschemeng.8b00282.
[15] Solmaz R, Döner A, Kardaş G. Electrochemical deposition and characterization of NiCu coatings as cathode materials for hydrogen evolution reaction. Electrochem Commun 2008;10:1909–11. http://dx.doi.org/10.1016/j.elecom.2008.10.011.
[16] Ahsan MA, Puente Santiago AR, Hong Y, Zhang N, Cano M, Rodriguez-Castellon E, Echegoyen L, Sreenivasan ST, Noveron JC. Tuning of trifunctional NiCu bimetallic nanoparticles confined in a porous carbon network with surface composition and local structural distortions for the electrocatalytic oxygen reduction, oxygen and hydrogen evolution reactions. J Am Chem Soc 2020;142:14688–701. http://dx.doi.org/10.1021/jacs.0c06960.
[17] Du M, Li X, Pang H, Xu Q. Alloy electrocatalysts. EnergyChem 2023;5:100083. http://dx.doi.org/10.1016/j.enchem.2022.100083.
[18] Etesami M, Mohamad AA, Nguyen MT, Yonezawa T, Pornprasertsuk R, Somwangthanaroj A, Kheawhom S. Benchmarking superfast electrodeposited bimetallic (Ni, Fe, Co, and Cu) hydroxides for oxygen evolution reaction. J Alloys Compd 2021;889:161738. http://dx.doi.org/10.1016/j.jallcom.2021.161738.
[19] Chen Z, Yun S, Wu L, Zhang J, Shi X, Wei W, Liu Y, Zheng R, Han N, Ni B-J. Waste-derived catalysts for water electrolysis: Circular economy-driven sustainable green hydrogen energy. Nano-Micro Lett 2023;15:1–37. http://dx.doi.org/10.1007/s40820-022-00974-7.
[20] Perdew JP, Burke K, Ernzerhof M. Generalized gradient approximation made simple. Phys Rev Lett 1996;77:3865–8. http://dx.doi.org/10.1103/physrevlett.77.3865.
[21] Kresse G, Hafner J. *Ab initio* molecular dynamics for open-shell transition metals. Phys Rev B 1993;48:13115–8. http://dx.doi.org/10.1103/physrevb.48.13115.
[22] Kresse G, Furthmüller J. Efficient iterative schemes for *Ab initio* total-energy calculations using a plane-wave basis set. Phys Rev B 1996;54:11169–86. http://dx.doi.org/10.1103/physrevb.54.11169.
[23] Grimme S, Antony J, Ehrlich S, Krieg H. A consistent and accurate *Ab initio* parametrization of density functional dispersion correction (DFT-D) for the 94 elements H–Pu. J Chem Phys 2010;132:154104. http://dx.doi.org/10.1063/1.3382344.

[24] Blöchl PE. Projector augmented-wave method. Phys Rev B 1994;50:17953–79. http://dx.doi.org/10.1103/physrevb.50.17953.

[25] Kresse G, Joubert D. From ultrasoft pseudopotentials to the projector augmented-wave method. Phys Rev B 1999;59:1758–75. http://dx.doi.org/10.1103/physrevb.59.1758.

[26] Jiao Y, Zheng Y, Jaroniec M, Qiao SZ. Design of electrocatalysts for oxygen- and hydrogen-involving energy conversion reactions. Chem Soc Rev 2015;44:2060–86. http://dx.doi.org/10.1039/C4CS00470A.

[27] Nørskov JK, Rossmeisl J, Logadottir A, Lindqvist L, Kitchin JR, Bligaard T, Jónsson H. Origin of the overpotential for oxygen reduction at a fuel-cell cathode. J Phys Chem B 2004;108:17886–92. http://dx.doi.org/10.1021/jp047349j.

[28] Peterson AA, Abild-Pedersen F, Studt F, Rossmeisl J, Nørskov JK. How copper catalyzes the electroreduction of carbon dioxide into hydrocarbon fuels. Energy Env Sci 2010;3:1311. http://dx.doi.org/10.1039/c0ee00071j.

[29] Larsen AH, Mortensen JJ, Blomqvist J, Castelli IE, Christensen R, Dułak M, Friis J, Groves MN, Hammer B, Hargus C, Hermes ED, Jennings PC, Jensen PB, Kermode J, Kitchin JR, Kolsbjerg EL, Kubal J, Kaasbjerg K, Lysgaard S, Maronsson JB, Maxson T, Olsen T, Pastewka L, Peterson A, Rostgaard C, Schiøtz J, Schütt O, Strange M, Thygesen KS, Vegge T, Vilhelmsen L, Walter M, Zeng Z, Jacobsen KW. The atomic simulation environment—a Python library for working with atoms. J Phys: Condens Matter 2017;29:273002. http://dx.doi.org/10.1088/1361-648X/aa680e.

[30] Neto MMCB, Moraes PIR, Da Silva JLF. Iridium-based materials as an electrocatalyst in computational investigation of their performance for hydrogen and oxygen evolution reactions. ACS Appl Energy Mater 2025;8:16947–63. http://dx.doi.org/10.1021/acsaem.5c02853.

[31] Turchanin MA, Agraval PG, Nikolaenko IV. Thermodynamics of alloys and phase equilibria in the copper-iron system. J Phase Equilib 2003;24:307–19. http://dx.doi.org/10.1361/105497103770330280.

[32] Li K, Fu C. Ground-state properties and lattice-vibration effects of disordered Fe–Ni systems for phase stability predictions. Phys Rev Mater 2020;4:023606. http://dx.doi.org/10.1103/PhysRevMaterials.4.023606.

[33] Mehl MJ, Hicks D, Toher C, Levy O, Hanson RM, Hart G, Curtarolo S. The AFLOW library of crystallographic prototypes: Part 1. Comput Mater Sci 2017;136:S1–828. http://dx.doi.org/10.1016/j.commatsci.2017.01.017.

[34] Barabash SV, Chepulskii RV, Blum V, Zunger A. First-principles determination of low-temperature order and ground states of Fe–Ni, Fe–Pd, and Fe–Pt. Phys Rev B 2009;80:220201. http://dx.doi.org/10.1103/PhysRevB.80.220201.

[35] Vitos L, Ruban AV, Skriver HL, Kollár J. The surface energy of metals. Surf Sci 1998;411:186–202. http://dx.doi.org/10.1016/S0039-6028(98)00363-X.

[36] Yu J, Lin X, Wang J, Chen J, Huang W. First-principles study of the relaxation and energy of bcc-Fe, fcc-Fe and AISI-304 stainless steel surfaces. Appl Surf Sci 2009;255:9032–9. http://dx.doi.org/10.1016/j.apsusc.2009.06.087.

[37] Karimadom BR, Sermiagin A, Meyerstein D, Zidki T, Mizrahi A, Bar-Ziv R, Kornweitz H. Hydrogen adsorption on various transition metal (111) surfaces in water: A DFT forecast. Phys Chem Chem Phys 2024;26:7647–57. http://dx.doi.org/10.1039/D3CP05884K.

[38] Allés M, Meng L, Beltrán I, Fernández F, Viñes F. Atomic hydrogen interaction with transition metal surfaces: A high-throughput computational study. J Phys Chem C 2024;128:20129–39. http://dx.doi.org/10.1021/acs.jpcc.4c06194.

[39] Xu L, Kirvassilis D, Bai Y, Mavrikakis M. Atomic and molecular adsorption on Fe(110). Surf Sci 2018;667:54–65. http://dx.doi.org/10.1016/j.susc.2017.09.002.

[40] Xu L, Lin J, Bai Y, Mavrikakis M. Atomic and molecular adsorption on Cu(111). Top Catal 2018;61:736–50. http://dx.doi.org/10.1007/s11244-018-0943-0.

[41] Bai Y, Kirvassilis D, Xu L, Mavrikakis M. Atomic and molecular adsorption on Ni(111). Surf Sci 2019;679:240–53. http://dx.doi.org/10.1016/j.susc.2018.08.004.

[42] Nørskov JK, Bligaard T, Logadottir A, Kitchin JR, Chen JG, Pandelov S, Stimming U. Trends in the exchange current for hydrogen evolution. J Electrochem Soc 2005;152:J23. http://dx.doi.org/10.1149/1.1856988.

[43] Greeley J, Nørskov JK. Large-scale, density functional theory-based screening of alloys for hydrogen evolution. Surf Sci 2007;601:1590–8. http://dx.doi.org/10.1016/j.susc.2007.01.037.

[44] Skúlason E, Karlberg GS, Rossmeisl J, Bligaard T, Greeley J, Jónsson H, Nørskov JK. Density functional theory calculations for the hydrogen evolution reaction in an electrochemical double layer on the Pt(111) electrode. Phys Chem Chem Phys 2007;9:3241–50. http://dx.doi.org/10.1039/B700099E.

[45] Santos E, Lundin A, Pötting K, Quaino P, Schmickler W. Model for the electrocatalysis of hydrogen evolution. Phys Rev B 2009;79:235436. http://dx.doi.org/10.1103/PhysRevB.79.235436.

[46] Santos HLS, Corradini PG, Medina M, Mascaro LH. Effect of copper addition on cobalt-molybdenum electrodeposited coatings for the hydrogen evolution reaction in alkaline medium. Int J Hydrog Energy 2020;45:33586–97. http://dx.doi.org/10.1016/j.ijhydene.2020.09.128.

[47] Zhang J, Xiao B, Liu X, Liu P, Xi P, Xiao W, Ding J, Gao D, Xue D. Copper dopants improved the hydrogen evolution activity of earth-abundant cobalt pyrite catalysts by activating the electrocatalytically inert sulfur sites. J Mater Chem A 2017;5:17601–8. http://dx.doi.org/10.1039/C7TA05433E.

[48] Lu Q, Hutchings GS, Yu W, Zhou Y, Forest RV, Tao R, Rosen J, Yonemoto BT, Cao Z, Zheng H, Xiao JQ, Jiao F, Chen JG. Highly porous non-precious bimetallic electrocatalysts for efficient hydrogen evolution. Nat Commun 2015;6:1–8. http://dx.doi.org/10.1038/ncomms7567.

[49] Gautier S, Steinmann SN, Michel C, Fleurat-Lessard P, Sautet P. Molecular adsorption at Pt(111). How accurate are DFT functionals? Phys Chem Chem Phys 2015;17:28921–30. http://dx.doi.org/10.1039/C5CP04534G.

[50] Bartaquim EO, Bezerra RC, Bittencourt AFB, Da Silva JLF. Computational investigation of van der Waals corrections in the adsorption properties of molecules on the Cu(111) surface. Phys Chem Chem Phys 2022;24:20294–302. http://dx.doi.org/10.1039/D2CP02663E.

[51] Quaino P, Juarez F, Santos E, Schmickler W. Volcano plots in hydrogen electrocatalysis – uses and abuses. Beilstein J Nanotechnol 2014;5:846–54. http://dx.doi.org/10.3762/bjnano.5.96.

[52] Govindarajan N, Kastlunger G, Gauthier JA, Cheng J, Filot I, Hagopian A, Hansen HA, Huang J, Kowalski PM, Liu J, Lombardi JM, Maraschin M, Peterson A, Pillai HS, Prats H, Price CJ, van Roij R, Rossmeisl J, Seemakurthi RR, Shin S-J, Smith A, Zhu J-X, Doblhoff-Dier K. The intricacies of computational electrochemistry. ACS Energy Lett 2025;10:4277–88. http://dx.doi.org/10.1021/acsenergylett.5c00748.

[53] Heenen HH, Gauthier JA, Kristoffersen HH, Ludwig T, Chan K. Solvation at metal/water interfaces: An *ab initio* molecular dynamics benchmark of common computational approaches. J Chem Phys 2020;152:144703. http://dx.doi.org/10.1063/1.5144912.

[54] Manz TA, Limas NG. Introducing DDEC6 atomic population analysis: Part 1. Charge partitioning theory and methodology. RSC Adv 2016;6:47771–801. http://dx.doi.org/10.1039/C6RA04656H.

[55] Limas NG, Manz TA. Introducing DDEC6 atomic population analysis: Part 2. Computed results for a wide range of periodic and nonperiodic materials. RSC Adv 2016;6:45727–47. http://dx.doi.org/10.1039/C6RA05507A.

[56] Hammer B, Nørskov JK. Electronic factors determining the reactivity of metal surfaces. Surf Sci 1995;343:211–20. http://dx.doi.org/10.1016/0039-6028(96)80007-0.

[57] Mavrikakis M, Hammer B, Nørskov JK. Effect of strain on the reactivity of metal surfaces. Phys Rev Lett 1998;81:2819–22. http://dx.doi.org/10.1103/PhysRevLett.81.2819.

[58] Da Silva JLF, Stampfl C. Trends in adsorption of noble gases He, Ne, Ar, Kr, and Xe on Pd(111)-$(3\times3)R30°$: All-electron density-functional calculations. Phys Rev B 2008;77:045401. http://dx.doi.org/10.1103/physrevb.77.045401.

[59] Arshad F, Tahir A, Haq Tu, Duran H, Hussain I, Sher F. Fabrication of NiCu interconnected porous nanostructures for highly selective methanol oxidation coupled with hydrogen evolution reaction. Int J Hydrog Energy 2022;47:36118–28. http://dx.doi.org/10.1016/j.ijhydene.2022.08.187.

[60] Wei C, Sun Y, Scherer GG, Fisher AC, Sherburne M, Ager JW, Xu ZJ. Surface composition dependent ligand effect in tuning the activity of nickel–copper bimetallic electrocatalysts toward hydrogen evolution in alkaline. J Am Chem Soc 2020;142:7765–75. http://dx.doi.org/10.1021/jacs.9b12005.

[61] Strmcnik D, Lopes PP, Genorio B, Stamenkovic VR, Markovic NM. Design principles for hydrogen evolution reaction catalyst materials. Nano Energy 2016;29:29–36. http://dx.doi.org/10.1016/j.nanoen.2016.04.017.

[62] Yutomo EB, Noor FA, Winata T. Surface stability and electronic structure of CuNi alloy (111) as a potential catalyst for graphene growth-a density-functional theory study. J Phys Conf Ser 2022;2243:012045. http://dx.doi.org/10.1088/1742-6596/2243/1/012045.

[63] Zhou Y, Wang Z, Pan Z, Liu L, Xi J, Luo X, Shen Y. Exceptional performance of hierarchical Ni–Fe (hydr)oxide@NiCu electrocatalysts for water splitting. Adv Mater 2019;31:1806769. http://dx.doi.org/10.1002/adma.201806769.

[64] Jiang W, Faid AY, Gomes BF, Galkina I, Xia L, Lobo CMS, Desmau M, Borowski P, Hartmann H, Maljusch A, Besmehn A, Roth C, Sunde S, Lehnert W, Shviro M. Composition-dependent morphology, structure, and catalytical performance of nickel–iron layered double hydroxide as highly-efficient and stable anode catalyst in anion exchange membrane water electrolysis. Adv Funct Mater 2022;32:2203520. http://dx.doi.org/10.1002/adfm.202203520.

[65] Campagna Zignani S, Faro ML, Carbone A, Italiano C, Trocino S, Monforte G, Aricò AS. Performance and stability of a critical raw materials-free anion exchange membrane electrolysis cell. Electrochim Acta 2022;413:140078. http://dx.doi.org/10.1016/j.electacta.2022.140078.

[66] Lopes PP, Chung DY, Rui X, Zheng H, He H, Farinazzo Bergamo Dias Martins P, Strmcnik D, Stamenkovic VR, Zapol P, Mitchell JF, Klie RF, Markovic NM. Dynamically stable active sites from surface evolution of perovskite materials during the oxygen evolution reaction. J Am Chem Soc 2021;143:2741–50. http://dx.doi.org/10.1021/jacs.0c08959.

[67] Wang Y, Xiao L, Li M, Zhang Y, Liu T. High-density defect-induced ultrahigh boron and nitrogen doping of iron–copper-functionalized porous carbon nanosheets for enhanced water splitting. J Phys Chem Solids 2024;186:111812. http://dx.doi.org/10.1016/j.jpcs.2023.111812.

[68] Lee S, Bai L, Hu X. Deciphering iron-dependent activity in oxygen evolution catalyzed by nickel–iron layered double hydroxide. Angew Chem Int Ed 2020;59:8072–7. http://dx.doi.org/10.1002/anie.201915803.

[69] Wang X, Jiang Z, Ma Y, Su X, Zhao X, Zhu A, Zhang Q. Ni/Fe based electrocatalyst for highly-efficient anion exchange membrane water electrolysis. J Power Sources 2024;591:233819. http://dx.doi.org/10.1016/j.jpowsour.2023.233819.

[70] Galkina I, Faid AY, Jiang W, Scheepers F, Borowski P, Sunde S, Shviro M, Lehnert W, Mechler AK. Stability of Ni–Fe-layered double hydroxide under long-term operation in AEM water electrolysis. Small 2024;20:2311047. http://dx.doi.org/10.1002/smll.202311047.

[71] da Cruz JC, Silva RMe, da Silva GTST, Mascaro LH, Ribeiro C. Recycling spent batteries to green innovation: A CuCo-based composite as an electrocatalyst for $CO_2$ reduction. Sustain Energy Fuels 2024;8:3104–12. http://dx.doi.org/10.1039/D4SE00368C.

[72] Almeida CVS, Mascaro LH. Enhancing electrochemical $N_2$ reduction at mild conditions with $Fe_xO_y$ co-deposited on amorphous $MoS_2$. Electrochim Acta 2024;476:143680. http://dx.doi.org/10.1016/j.electacta.2023.143680.

[73] Gonçalves CB, da Silva RT, Dalenogare G, Gonzaga IMD, Mascaro LH, Ferrer MM, Assis M, Longo E, de Carvalho HB, Doriguetto AC. Comprehensive experimental and theoretical studies on the synthesis and characterization of electrodeposited nanostructured $Cu_2O$ thin films. Surf Interfaces 2023;42:103397. http://dx.doi.org/10.1016/j.surfin.2023.103397.

[74] Zheng X, Qin M, Ma S, Chen Y, Ning H, Yang R, Mao S, Wang Y. Strong oxide-support interaction over $IrO_2/V_2O_5$ for efficient pH-universal water splitting. Adv Sci 2022;9:2104636. http://dx.doi.org/10.1002/advs.202104636.

[75] Vasileff A, Zhi X, Xu C, Ge L, Jiao Y, Zheng Y, Qiao S-Z. Selectivity control for electrochemical $CO_2$ reduction by charge redistribution on the surface of copper alloys. ACS Catal 2019;9:9411–7. http://dx.doi.org/10.1021/acscatal.9b02312.